Ore Geology Reviews 136 (2021) 104253

Contents lists available at ScienceDirect

Ore Geology Reviews

journal homepage: www.elsevier.com/locate/oregeorev

LA-ICP-MS sphalerite and galena trace element chemistry and mineralization-style fingerprinting for carbonate-hosted Pb-Zn deposits: Perspective from early Devonian Huodehong deposit in Yunnan, South China

Yusi Hu [a,b], Chen Wei [a,b], Lin Ye [a,*], Zhilong Huang [a,*], Leonid Danyushevsky [c,d], Haoyu Wang [a,b]

[a] State Key Laboratory of Ore Deposit Geochemistry, Institute of Geochemistry, Chinese Academy of Sciences, Guiyang 550081, China
[b] University of Chinese Academy of Sciences, Beijing 100049, China
[c] Centre for Ore Deposit and Earth Sciences (CODES), University of Tasmania, Private Bag 79, TAS 7001, Australia
[d] Transforming the Mining Value Chain (TMVC), Australian Research Council (ARC) Industrial Transformation Research Hub, University of Tasmania, Hobart, TAS 7001, Australia

ARTICLE INFO

Keywords:
Trace elements
Sphalerite
Galena
Mineralization temperature, Ore genesis,
Sichuan-Yunnan-Guizhou Pb-Zn metallogenic province (SYGMP)
Mississippi Valley-type (MVT) Pb-Zn deposits

ABSTRACT

The Sichuan-Yunnan-Guizhou metallogenic province (SYGMP) in the southwestern margin of the Yangtze block is an important Pb-Zn province in China. In the SYGMP, over 400 Pb-Zn deposits are mostly hosted in the Sinian, Lower Cambrian and Carboniferous sedimentary rocks and rarely in the Devonian carbonate rocks (e.g., Houdehong). For Houdehong, however, its ore-forming conditions and deposit type remain unclear due to limited geological and geochemical data available. In this study, LA-ICP-MS spot analysis and mapping were conducted to determine the trace element features in the sphalerite and galena from Huodehong. The results show that the sphalerite is characterized by enrichments in Ge and Tl but depletions of Fe, Mn, and Co. Most of these elements have widely varying concentrations and occur as solid solutions in the sphalerite crystal lattice. The critical element of Ge enters sphalerite through coupling substitution with Mn^{2+} for Zn^{2+} and/or Cd^{2+}. The results calculated by empirical formula show that the sphalerite mineralization occurred under low-temperature conditions (<180°C). Meanwhile, the Houdehong galena contains low Se, Cd, Tl and Bi, and very low Ag (<1.0 ppm) and Sb (<5.0 ppm) concentrations, which is likely controlled by the original ore-fluid compositions. Trace element compositions of the Houdehong sulfides are generally similar to that of the sulfides from Mississippi Valley-type (MVT) deposits and many other Pb-Zn deposits in the SYGMP, but markedly different from those of volcanogenic massive sulfide (VMS), sedimentary exhalative (SEDEX) and skarn Pb-Zn deposits. Considering also the deposit geological and geochemical features, we considered that the Huodehong Pb-Zn deposit is of MVT. Our findings provide further geological and geochemical evidence for understanding the Devonian carbonate-hosted Pb-Zn mineralization in the region.

1. Introduction

The Sichuan-Yunnan-Guizhou Pb-Zn metallogenic province (SYGMP) is an important constituent of the giant Mesozoic South China low-temperature metallogenic domain, and supplies considerable amounts of Pb-Zn-Ag and other mineral resources (Zhang et al., 2005, 2015; Hu and Zhou, 2012; Zhou et al., 2018). The SYGMP encompasses a total area of about 170,000 km^2, and hosts over 400 Pb-Zn deposits of different scales, which are distributed in clusters or along belts (Liu and Lin, 1999). Among these deposits, over 62% are hosted in the Sinian-Lower Cambrian and Carboniferous carbonate sequences, accounting for 70% of the total Pb-Zn resource in the SYGMP (Wu, 2013). Extensive metallogenic studies have been conducted on these Carboniferous and Sinian-Lower Cambrian dolostone-hosted (e.g., Huize, Tanbaoshan, Maozu, Dalingzi, Wusihe) deposits, to document their geological characteristics, genesis of ores, timing of mineralization and tectonic setting (e.g., Huang et al., 2004; Han et al., 2007; Zhang et al., 2015; Ye et al., 2016; Xiong et al., 2018; Yuan et al., 2018; Zhou et al., 2018 and

* Corresponding authors.
E-mail addresses: yelin@vip.gyig.ac.cn (L. Ye), huangzhilong@vip.gyig.ac.cn (Z. Huang).

https://doi.org/10.1016/j.oregeorev.2021.104253
Received 11 December 2020; Received in revised form 9 May 2021; Accepted 22 May 2021
Available online 25 May 2021

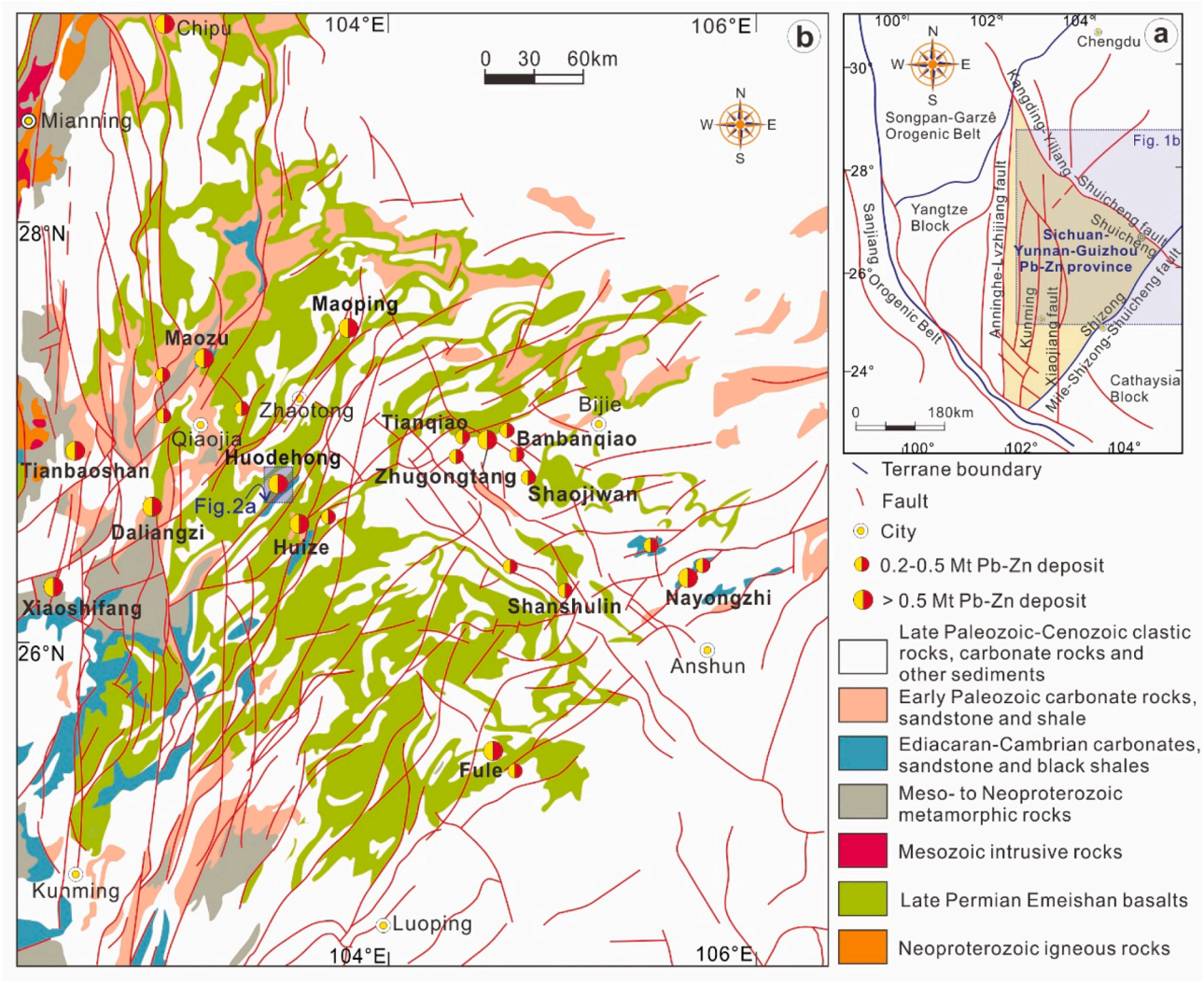

Fig. 1. (a) Regional tectonic geological setting of Sichuan-Yunnan-Guizhou metallogenic province (SYGMP); (b) Geologic map of the SYGMP showing the distribution of Pb-Zn deposits Strata, Emeishan basalts and faults (modified from Huang et al., 2004; Zhou et al., 2018).

references therein). For instance, several ore genetic models have been proposed, including the sedimentary exhalative (SEDEX; Jin et al., 2016), sedimentary reworking-type (e.g., Liu and Lin 1999), Emeishan large igneous province (ELIP)-related (e.g., Huang et al., 2001; Xu et al., 2014), Mississippi Valley-type (MVT; e.g., Zhang et al., 2005, 2015; Ye et al., 2011, 2016; Wei et al., 2021) and SYG- or HZ-type which is different from typical MVT (e.g., Han et al., 2007, 2012; Zhou et al., 2013a, 2013b, 2018). However, to date their Devonian carbonate-hosted counterparts remain poorly investigated and understood.

The Devonian carbonate-hosted Huodehong deposit at the middle SYGMP (Fig. 1) hosts ~3.0 Mt sulfide ores @ 6.38% Zn and 0.97% Pb (Wang, 2010). Despite its economic significance, only limited S-Pb isotope data of the deposit have been published in local Chinese literature (e.g., Jin et al., 2016; Wu et al., 2016). Published Pb isotope data of sulfides are similar to that of the basement rocks, suggesting a metamorphic basement-derived metal source (Jin et al., 2016; Wu et al., 2016). Whilst sulfide S-isotope data reflect the depletion of $\delta^{34}S$ (-16.6 – −10.4‰) in hydrothermal fluid, a typical characteristic of biogenic sulfur. The S isotopic signatures are comparable to the $\delta^{34}S$ value of hydrothermal fluid (-17.5 – −8.5‰) generated by the bacterial sulfate reduction of Devonian evaporitic sulfates, indicating the reduced sulfur was derived from evaporitic sulfates within ore-hosting strata via BSR (Wu et al., 2016). Due to the limited geological and geochemical studies, many metallogenic questions on Huodehong, in particular the mineralizing conditions and ore genesis, remain unanswered.

Sphalerite is a key ore mineral in Pb-Zn deposits, and contains a variety of trace elements (including Fe, Cd, Co, In, Mn, Ge, Ga, Ag), which are widely used to decipher the physicochemical conditions of hydrothermal fluid evolution and discriminate the Pb-Zn metallogenetic types (e.g., Di Benedetto et al., 2005; Kelley et al., 2004; Ye et al., 2011; Belissont et al., 2014; Frenzel et al., 2016; Wei et al., 2019). Complex mineral texture, such as compositional zoning and fine intergrowth, are common in the Houdehong sphalerite (Jin et al., 2016), electron microprobe (EMP), scanning electron microscopy (SEM) and/or wet chemistry cannot provide accurate results (low detection limit) for trace elements and isotopes at the micro-scale. Recent advances micro-analytical techniques (e.g., LA-ICPMS and SIMS) could resolve the spatial geochemical information recorded in these complex textural features. For example, LA-ICP-MS enables accurate (low detection limit) and high spatial-resolution concentration measurements for elements and isotopes (e.g., Cook et al., 2009; Ye et al., 2011), and has been widely adopted to constrain the trace element compositions of sulfides from different types of deposits (e.g., Cook et al., 2011; Ye et al., 2012, 2016; Ciobanu et al., 2013; George et al., 2015, 2016).

In this paper, LA-ICP-MS trace-element spot analysis and mapping were performed on the sphalerite and galena from the Huodehong Pb-Zn deposit, with the aims to (i) determine the mode of trace-element occurrence in sulfides; (ii) constrain the trace-elements (Sb and Ag)

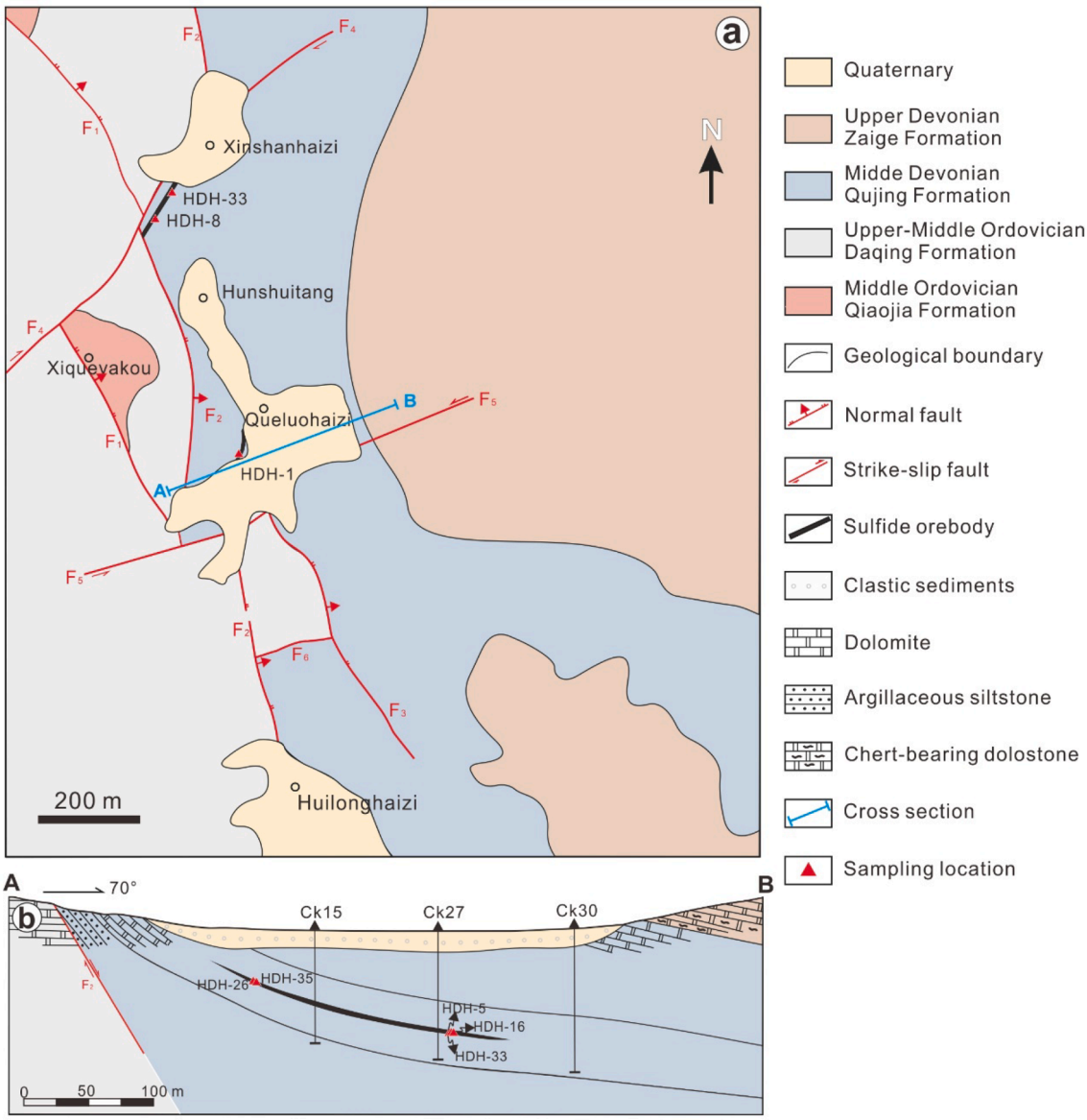

Fig. 2. (a) Geologic map of the Huodehong Pb-Zn deposit (modified from Wu et al., 2016); (b) cross-section A-B through the Huodehong mine area (modified from Wu et al., 2016).

behavior in galena, (iii) constrain the sulfide mineralization temperature; and (iv) reveal the ore deposit type and genesis of the Houdehong deposit. Our findings will provide new geochemical evidence for understanding the Devonian carbonate-hosted Pb-Zn mineralization in the SYGMP.

2. Regional geology

The Sichuan-Yunnan-Guizhou tringle district, located within the southwestern margin of the Yangtze Block (Fig. 1a), is confined by the NW-trending Weining-Shuicheng, the SN-trending Anninghe and the NE-trending Mile-Shizhong regional fault belts (Fig. 1b). These three belts extend deep into basement rocks and have been activated and reactivated by a series of tectonic events, such as the Hercynian, Indosinian, Yanshanian and Himalayan orogenic events. A set of secondary NE-trending and NW-trending faults and thrust faults are well developed in the district.

Regional stratigraphy comprises a Mesoproterozoic to Early Neoproterozoic folded basement overlain by middle Neoproterozoic weakly metamorphosed strata, late Neoproterozoic unmetamorphosed Sinian, and Phanerozoic cover. The folded basement is mainly composed of greywacke, slate, siltstone, slate, shale, dolostone and minor tuffaceous volcanic rocks (Yan et al., 2003). The over successions include Neoproterozoic to the middle Triassic submarine carbonate and clastic sedimentary sequences and Jurassic to Cenozoic continental sedimentary rocks as well as the Upper Permian Emeishan flood basalt. Evaporitic sulfate is commonly in the Sinian to Triassic marine sedimentary strata, which is the important sulfur source of the sedimentary-hosted hydrothermal deposit in the South China Block (e.g., Zhou et al., 2013a, Zhou et al., 2018).

The SYGMP hosts a great number of Pb-Zn deposits in different scales, which is hosted within the Sinian to early Permian carbonate strata (Liu and Lin, 1999; Huang et al., 2004; Zhang et al., 2005). The deposits are characterized by fault-controlled orebodies, simple mineral assemblage (sphalerite, pyrite, galena, calcite with minor quartz), weak wall rock alteration, and high ore grade (15–35 wt%) of Pb and Zn associated with the enrichment of Ag, Ge, Cd, Ga, and In. Recent Sm-Nd dating hydrothermal calcite/fluorite and Rb-Sr dating sphalerite indicate that the carbonate-hosted Pb-Zn deposits have a peak age of 226–192 Ma, implying the Pb-Zn mineralization in the SYG district is

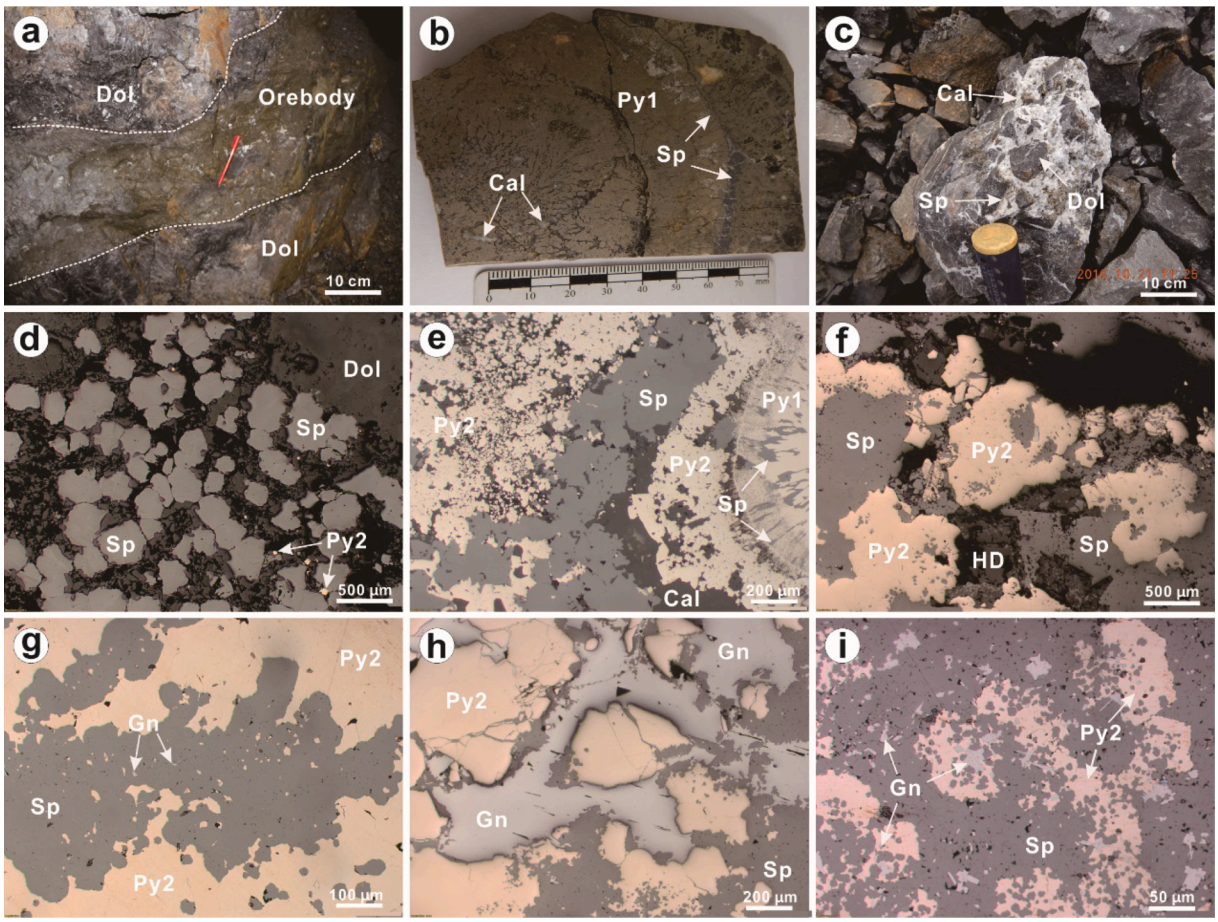

Fig. 3. Photographs of the sulfide ores from the Huodehong deposit; (a) Stratiform orebody; (b) Sphalerite veinlet in colloform pyrite ore; (c) Sphalerite and calcite cement the dolostone breccias. (d) Disseminated sphalerite in dolomite; (e) Colloform pyrite (Py1) replaced by sphalerite, which is in turn replaced by late xenomorphic pyrite (Py2); (f) Sphalerite with fine galena inclusions was replaced by xenomorphic pyrite (Py2); (h) xenomorphic pyrite (Py2) and sphalerite replaced by galena; (i) Xenomorphic pyrite (Py2) replaced by sphalerite and galena. Abbreviations: Sp–sphalerite, Py1–pre ore stage colloidal pyrite, Py2–early ore stage xenomorphic pyrite, Dol–dolomite, Cal–calcite.

likely related to the Indosinian orogenic event (e.g., Lin et al., 2010; Hu and Zhou, 2012; Zhou et al., 2013b, 2018; Zhang et al., 2015).

3. Geology of Huodehong deposit

The Huodehong Pb-Zn deposit is located at the middle part of the Yangtze block (Fig. 1; Jin et al., 2016; Wu et al., 2016). Exposed stratigraphy at Huodehong include (Fig. 2): (i) Upper Ordovician Qiaojia Formation (Fm.) yellowish-green/dark-gray (silty-)mudstone and fine arkose; (ii) Middle-Upper Ordovician Daqing Fm. gray fine-crystalline dolostone with irregular silicic-argillaceous nodules at the top; (iii) Middle Devonian Qujing Fm. (unconformably overlies the Daqing Fm.) argillaceous siltstone and dolostone (118 m thick); (iv) Upper Devonian Zaige Fm. (conformity overlies the Qujing Fm.) gray medium-thick-bedded dolostone with minor iron-bearing argillaceous dolostone and chert; (v) Quaternary sediments. At Huodehong, the Qujing Fm. comprises three members, i.e., a lower member of argillaceous siltstone with silty mudstone, a middle member of light–dark gray coarse-crystalline dolostone (main ore host), and an upper member composed by argillaceous dolostone (Fig. 2b).

Structures at Huodehong are dominated by NS- and ENE-trending faults (Fig. 2a), and minor folds and interlayer fracture zones (Fig. 2a). The steep (75°) NS-trending regional normal fault (F_2) is located at western Huodehong, and is separated into three parts (Fig. 2a) by the ENE-trending strike-slip faults (F_4 and F_5). Previous studies interpreted that F_2 fault is an important ore-fluid channel at Huodehong (Jin et al., 2016; Wu et al., 2016).

The Huodehong Pb-Zn orebodies are lenticular or stratabound by the Qujing Fm. dolostone, and is divided into three sections by the F_4 and F_5 faults (Fig. 2b). Sulfide orebodies strike ENE and gently (6–15°) dip N. The orebodies are 0.30–5.81 m wide (avg. 3.08 m), 830–1200 m long (avg. 1080 m), and 0.7–3.73 m thick, and contain 0.50–3.96% Pb and 0.16–15.52% Zn.

The Huodehong Pb-Zn ores can be divided into the sulfide-dominated and oxide-dominated types, with the former accounting for 75% of the total reserve. Metallic minerals include mainly sphalerite (dominant), galena and pyrite with minor limonite. Non-metallic minerals comprise dominantly hydrothermal dolomite and calcite. The ores occur mainly as massive (Fig. 3a-b), brecciated (Fig. 3c), or disseminated (Fig. 3d), with major textures including oolitic/framboidal (Fig. 3b,e), xenomorphic-subhedral granular (Fig. 3c-i), metasomatic relict (Fig. 3e-i), and micro-band. For instance, metasomatic relict-textured sphalerite replaced oolitic/framboidal pyrite (termed Py1 in this study; Fig. 3e), whilst subhedral pyrite (termed Py2 in this study; Fig. 3f-i) or replaced subhedral galena and anhedral sphalerite (Fig. 3h-i). Wallrock alteration at Huodehong is well developed, and includes mainly pyritization (Fig. 3a) and dolomitization (Fig. 3c).

Based on detailed field geology, hand-specimen and thin-section microscopic observations, the mineral paragenetic sequence can be divided into four mineralization stages, including pre-ore satge (syngenetic sedimentary) colloform pyrite (Py1) → early-ore stage (hydrothermal stage) xenomorphic pyrite (Py2) → main-ore stage (sphalerite

Table 1
Trace elements in sulfides from the Huodehong Pb-Zn deposit (ppm).

Mineral		Mn	Fe	Co	Ni	Cu	Zn	Ge	As	Se	Ag	Cd	In	Sn	Sb	Te	Pt	Au	Tl	Pb	Bi
HDH-17, Level 2190 *m*																					
Sphalerite	Min	<0.44	85.2	<0.01	<0.05	13.5	–	0.86	<0.49	<0.93	1.68	4304	0.01	0.07	<0.04	0.23	<0.01	<0.01	<0.01	3.12	<0.01
	Max	5.27	675	0.04	<0.24	184	–	52.1	0.80	3.06	24.6	9875	0.84	12.6	<0.09	0.32	0.03	0.02	0.88	248	0.01
	Median(11)	3.38	174	0.03	–	91.3		19.5	0.80	1.91	2.16	6140	0.04	0.72	–	0.27	–		0.25	26.7	0.01
	Mean(11)	–	210	0.03	–	86	–	21.3	2.31	–	6.12	6321	0.14	2.20	–	0.27	–	–	0.33	49.4	–
	S.D.	–	163	0.01	–	50	–	15.5	0.77	–	7.29	1421	0.27	3.84	–	0.03	–	–	0.24	71.7	–
HDH-26, Level 2190 *m*																					
Sphalerite	Min	8.45	310	<0.02	<0.05	2.85	–	95.2	1.18	<0.99	1.94	1884	<0.003	<0.04	0.23	<0.19	<0.01	<0.02	2.46	450	0.01
	Max	16.7	882	0.06	0.27	7.73	–	140	3.68	<1.58	3.66	2312	0.01	0.18	1.05	0.31	0.02	0.09	5.37	1970	0.03
	Median(11)	10.0	542	0.04	0.19	5.84	–	103	2.32	–	2.93	2076	0.01	0.11	0.66	0.26	–	0.06	4.70	513	0.02
	Mean(11)	11.0	533	0.04	0.19	5.45	–	107	2.31	–	2.84	2085	0.01	0.12	0.60	0.26	–	0.06	4.13	742	0.02
	S.D.	2.38	181	0.01	0.10	1.68	–	12.4	0.77	–	0.49	116	0.003	0.04	0.27	0.06	–	0.02	1.08	457	0.01
HDH-35, Level 2190 *m*																					
Sphalerite	Min	39.4	634	<0.01	<0.07	1.46	–	260	<0.53	<0.97	1.34	1228	<0.003	<0.06	<0.05	<0.21	<0.01	<0.01	25.5	1207	<0.01
	Max	376	6421	0.06	0.27	11.0	–	451	3.01	2.42	2.03	2014	0.02	0.16	0.15	0.55	<0.05	<0.03	221	4789	<0.02
	Median(15)	204	1621	0.03	0.12	4.45	–	364	1.62	–	1.68	1683	0.01	0.10	0.12	0.27	–	–	152	3097	–
	Mean(15)	208	2550	0.04	0.17	5.45	–	357	1.80	–	1.70	1661	0.01	0.11	0.12	0.32	–	–	131	2842	–
	S.D.	114	2019	0.02	0.08	3.06	–	50.5	0.70	–	0.20	194	0.01	0.03	0.03	0.10	–	–	62.5	1092	–
HDH-1, Level 2150 *m*																					
Sphalerite	Min	15.9	814	0.01	<0.01	4.81	–	139	2.15	<1.09	1.84	1150	<0.003	0.17	0.79	<0.26	<0.02	0.06	8.58	807	<0.01
	Max	43.6	1123	0.09	0.23	15.7	–	183	4.42	1.82	2.35	1398	0.02	0.57	1.02	0.31	<0.05	0.15	15.2	1678	0.02
	Median(11)	21.0	912	0.04	0.17	6.52		173	3.07	1.82	2.00	1276	0.01	0.32	0.88	0.29	–	0.09	10.6	1030	–
	Mean(11)	26.3	961	0.04	0.15	7.54	–	166	3.30	–	2.06	1275	0.01	0.34	0.89	0.29	–	0.10	11.6	1164	–
	S.D.	9.45	131	0.02	0.06	3.18	–	13.7	0.75	–	0.17	68.5	0.01	0.12	0.08	0.03	–	0.03	2.48	306	–

Minerals		Mn	Fe	Co	Ni	Cu	Zn	Ge	As	Se	Ag	Cd	In	Sn	Sb	Te	Pt	Au	Tl	Pb	Bi
HDH-8, Level 2150*m*																					
Sphalerite	Min	71.2	407	<0.01	<0.05	1.22	–	93.8	<0.59	<1.08	1.29	495	0.003	2.94	<0.06	<0.22	<0.02	<0.01	12.1	160	<0.01
	Max	375	1383	<0.05	1.19	3.10	–	662	6.10	3.07	1.92	1296	0.023	12.9	<0.09	0.43	<0.07	<0.03	250	668	<0.02
	Median(8)	234	839	–	–	1.47	–	313	1.58	2.35	1.50	666	0.001	4.57	–	–	–	–	93.8	304	–
	Mean(8)	228	898	–	–	1.69	–	340	2.62	2.42	1.54	744	0.004	5.62	–	–	–	–	110	336	–
	S.D.	117	358	–	–	0.63	–	173	2.34	0.48	0.18	245	0.008	3.24	–	–	–	–	81.2	166	–
HDH-16, Level 2150*m*																					
Sphalerite	Min	6.79	449	<0.01	<0.11	2.22	–	1.10	<0.70	<1.09	1.42	1708	<0.01	<0.06	<0.05	<0.34	<0.01	<0.02	3.59	10.1	<0.01
	Max	58.0	6727	0.10	0.89	10.1	–	169	2.14	<1.75	2.40	3083	0.09	0.24	0.14	<0.54	0.03	<0.06	29.0	2442	<0.02
	Median(10)	43.7	719	0.04	0.31	7.50	–	127	1.44	–	1.88	2304	0.02	0.22	–	–	–	–	12.8	1301	–
	Mean(10)	40.8	1366	0.05	0.38	6.92	–	107	1.51	–	1.83	2279	0.04-	0.19	–	–	–	–	14.6	1374	–
	S.D.	14.2	1916	0.03	0.25	2.39	–	58.8	0.33	–	0.29	396	0.04-	0.06	–	–	–	–	8.52	916	–
Galena	Min	<0.18	<2.52	<0.01	<0.04	<0.05	<0.38	<0.14	<0.31	10.1	<0.01	15.3	<0.001	0.03	0.15	<0.12	<0.01	<0.01	9.50	–	0.03
	Max	1.03	349	<0.02	0.15	0.27	1075	0.50	<0.72	166	<0.03	81.2	<0.005	0.07	0.31	<0.35	<0.03	<0.04	29.9	–	0.37
	Median(8)	0.71	176	–	0.15	0.20	1.00	0.23	0.50	138	–	19.0	–	0.04	0.19	–	–	–	11.2	–	0.07
	Mean(8)	–	–	–	–	0.18	359	0.27	–	121	–	30.3	–	0.05	0.21	–	–	–	13.2	–	0.11
	S.D.	–	–	–	–	0.10	620	0.12	–	50.8	–	22.8	–	0.01	0.06	–	–	–	6.76	–	0.11
HDH-33, Level 2150*m*																					
Sphalerite	Min	1.17	458	<0.01	<0.05	0.65	–	1.78	<0.51	<1.09	1.32	799	0.01	<0.05	<0.05	<0.21	<0.01	<0.02	0.12	1.05	<0.01
	Max	139	4957	0.16	4.50	11.6	–	225	5.41	10.67	2.03	1990	0.15	13.21	<0.12	0.36	<0.05	<0.07	13.3	3722	<0.02
	Median(12)	54.6	2206	0.04	0.31	4.75	–	28.2	0.97	2.81	1.46	1366.7	0.02	0.38	–	0.32	–	–	6.25	220	–
	Mean(12)	56.6	2540	0.06	1.32	5.14	–	62.5	2.08	4.80	1.53	1310	0.04	1.94	–	0.26	–	–	6.33	782	–
	S.D.	43.0	1156	0.06	1.85	3.25	–	79.4	1.93	3.60	0.22	392	0.04	4.03	–	0.14	–	–	5.07	1174	–
HDH-5, Level 2150*m*																					
Galena	Min	<0.19	<2.19	<0.01	<0.02	<0.04	<0.39	<0.13	<0.27	0.87	<0.01	3.79	<0.001	0.03	0.46	<0.08	<0.01	<0.01	3.72	–	0.02
	Max	<0.28	<3.68	<0.02	0.03	<0.08	<0.68	0.23	0.72	13.2	0.01	10.0	<0.002	0.04	16.6	<0.29	<0.02	<0.02	8.24	–	0.44
	Median(8)	–	–	–	–	–	–	0.20	0.36	5.61	0.01	6.74	–	0.03	1.23	–	–	–	5.29	–	0.03
	Mean(8)	–	–	–	–		–	–	–	6.02	–	6.62	–	0.03	3.29	–	–	–	5.35	–	0.09
	S.D.	–	–	–	–		–	–	–	4.01	–	1.90	–	0.00	5.50	–	–	–	1.35	–	0.14

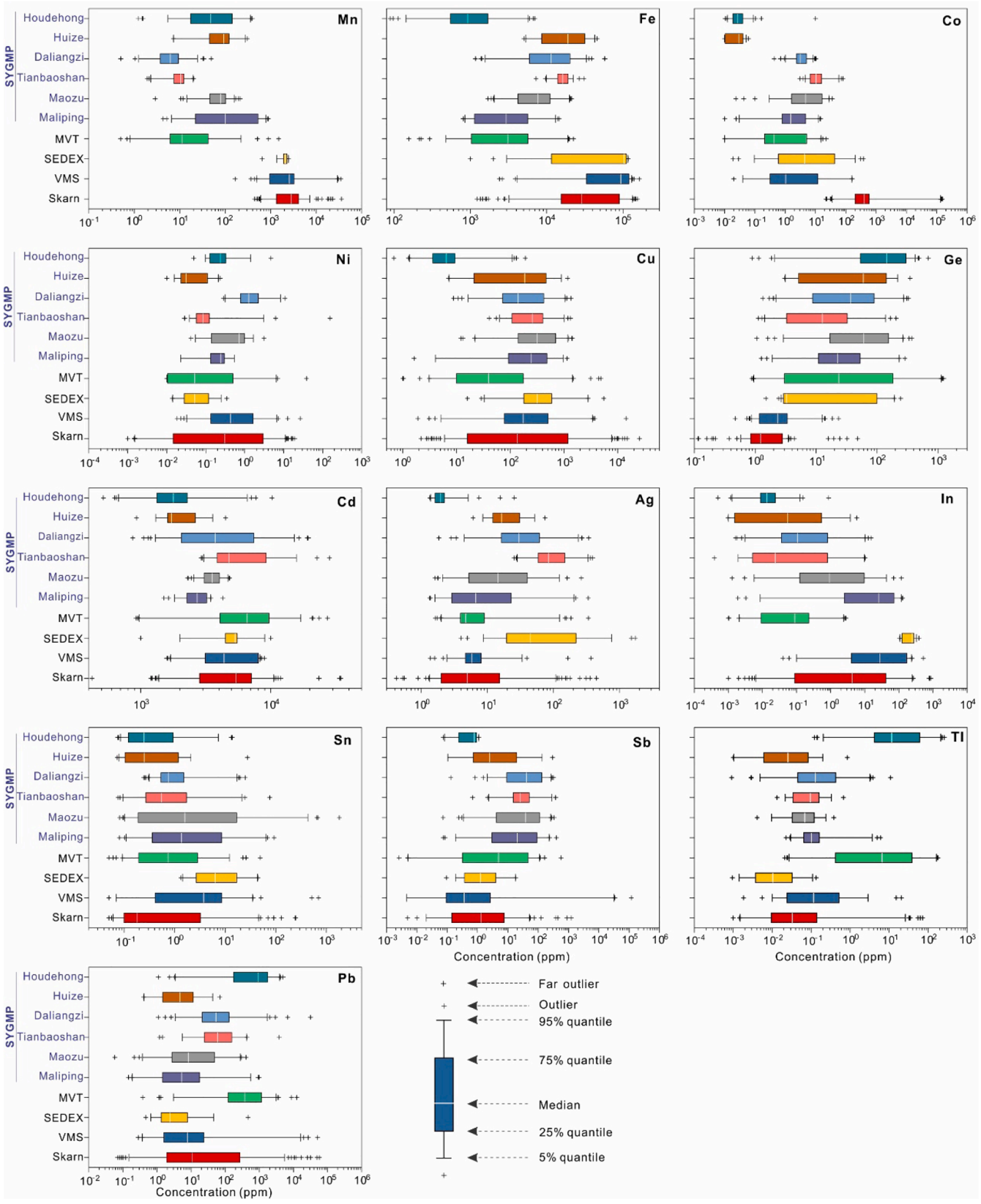

Fig. 4. Box and whisker plots of trace elements in sphalerite from Houdehong, other SYGMP Pb-Zn deposits, and major types of Pb-Zn deposits. Data of the SYGMP Pb-Zn deposits include Huize (Ye et al., 2011), Tianbaoshan (Ye et al., 2016), Daliangzi (Yuan et al., 2018); Maliping (Hu et al., 2019), Maozu (Li et al., 2020), and. Data of skarn, VMS, SEDEX and MVT deposits are from Cook et al. (2009), Ye et al. (2011), Bonnet et al. (2016), and Hu, (2020).

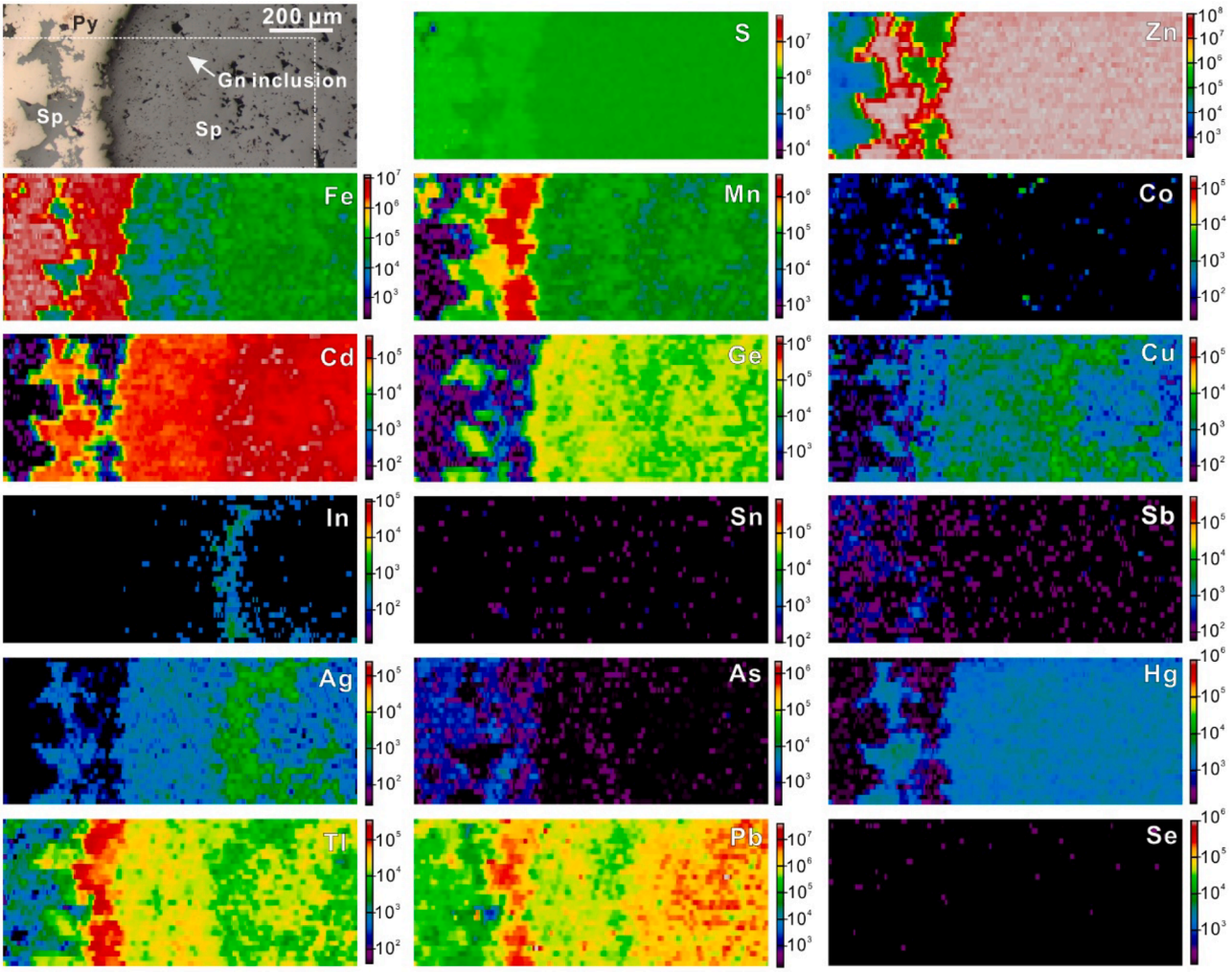

Fig. 5. LA-ICPMS elemental maps of sample HDH-35 from Huodehong.

+ galena) → late-ore stage (hydrothermal dolomite and calcite).

4. Samples and analytical methods

The Pb-Zn ore samples (7 sphalerite and 2 galena) were collected from level 2190 m and 2150 m mine tunnel at Huodehong (Table 1; Fig. 2). The samples were prepared into 1-inch polished slabs. Coarse mineral grains and the areas free of visible cracks or inclusions were selected for the LA-ICP-MS analysis (Table 1). Optical microscopy and scanning electron microscopy (SEM) backscattered electron (BSE) imaging were used to characterize the compositional inhomogeneity (e.g., zoning) and mineral inclusions, which would have affected the trace element distributions. Detailed LA-ICP-MS instrumentation and analytical procedures followed those given in Cook et al. (2009) and Ye et al. (2011).

LA-ICP-MS spot analysis and mapping were performed with an Agilent 7700 Quadrupole ICP-MS instrument attached to a high-performance RESOlution 193 nm ArF excimer laser ablation system at CODES (University of Tasmania, Australia). We used a consistent 30 μm-diameter spot size for all the analyses, which include 78 spots of sphalerite, 16 spots of galena, and one elemental map. Each analysis was performed in the time-resolved mode, which involves sequential peak hopping through the mass spectrum. The laser system was operated at a consistent 5 Hz pulse rate, with laser energy of 2.7 J/cm^2. Each laser pulse (ablation rate: 3.0 μm/sec) ablated ~ 0.3 μm depth of the samples. The following isotopes were monitored: ^{23}Na, ^{24}Mg, ^{27}Al, ^{29}Si, ^{39}K, ^{43}Ca, ^{49}Ti, ^{51}V, ^{53}Cr, ^{55}Mn, ^{57}Fe, ^{59}Co, ^{60}Ni, ^{65}Cu, ^{66}Zn, ^{72}Ge, ^{75}As, ^{77}Se, ^{90}Zr, ^{93}Nb, ^{95}Mo, ^{107}Ag, ^{111}Cd, ^{115}In, ^{118}Sn, ^{121}Sb, ^{125}Te, ^{157}Gd, ^{178}Hf, ^{181}Ta, ^{182}W, ^{195}Pt, ^{197}Au, ^{202}Hg, ^{205}Tl, ^{208}Pb ^{209}Bi, ^{232}Th and ^{238}U. Analysis time for each sample comprises 30 s laser-off background measurement and 60 s laser-on sample analysis. Acquisition time for each mass was set to 0.005–0.020 sec, with a total sweep time of ~0.07 sec. Data reduction was undertaken using Zn as the internal standard for sphalerite and Pb for galena. Average Pb and Zn concentrations for each sample were taken from EPMA measurements.

Calibration was performed with the in-house standard (STDGL2b-2) of powdered sulfides doped with certified element solutions and fused to a lithium borate glass disc. This standard is suitable for quantitative analyses in different sulfide matrixes (Danyushevsky et al., 2011). Empirical correction factors were applied to the measured ppm values in each sphalerite analysis as follows: Mn 1.46, Fe 1.49, Co 1.51, Ni 1.59, Cu 1.53, As 1.36, Se 1.85, Mo1.62, Ag 1.40, Cd 1.50, In 1.45, Sn 1.6, Sb 1.17, Te 1.00, Au 1.40, Tl 2.17, Pb 1.37, Bi 1.33 (Danyushevsky et al., 2011). These correction factors have been established by analyzing sphalerite secondary standards using STDGL2b2 and reflect the significant elemental fractionation between Zn and the other elements during ablation. The error on the correction factors is <5%. Analytical accuracy is better than 20%. No additional corrections were necessary for the galena analysis.

Raw analytical data for each spot analysis is plotted as a line graph and the integration times for background and sample signal selected. The counts were then corrected for instrumental drift (standards

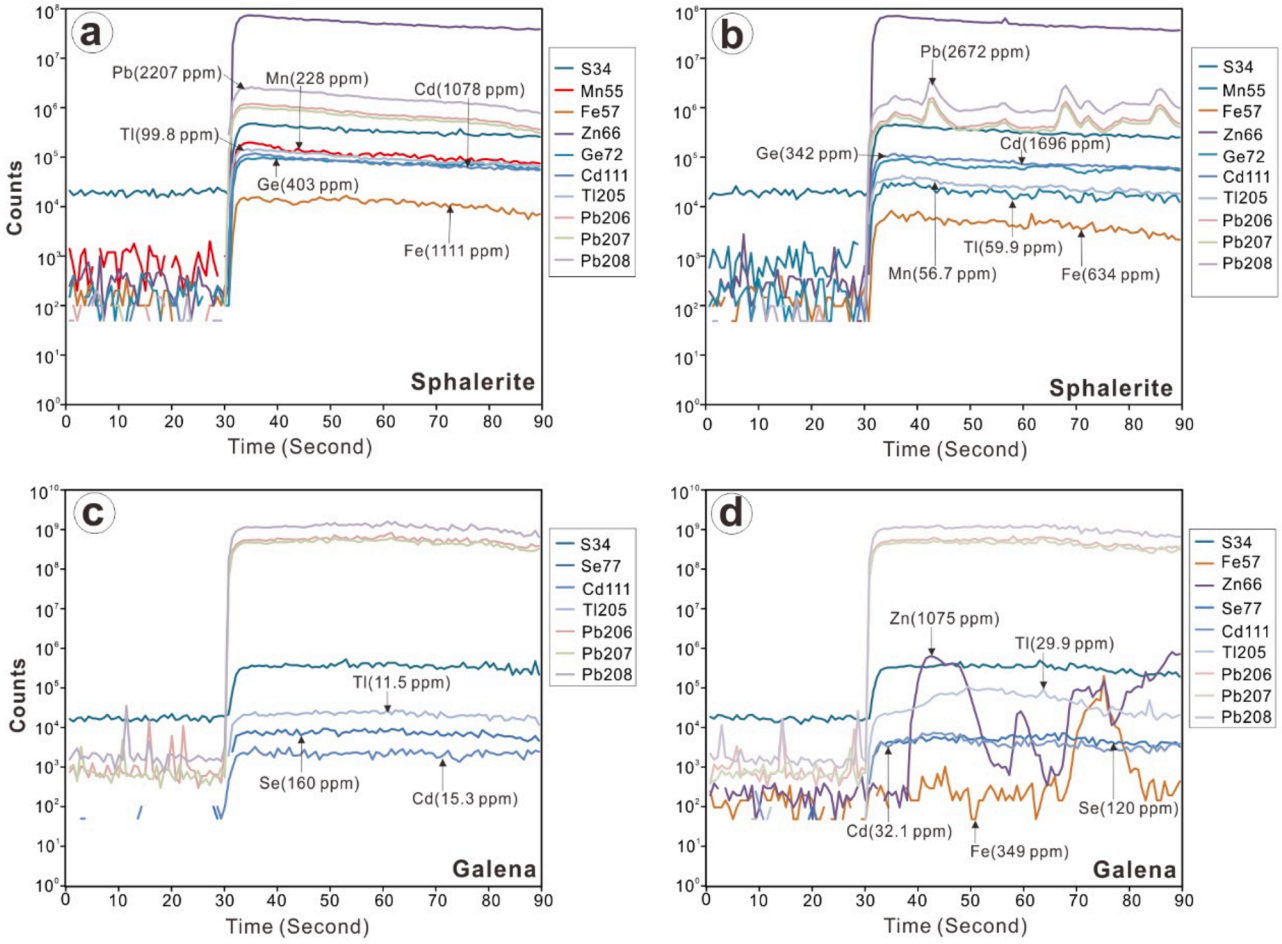

Fig. 6. Time-resolved LA-ICPMS signal depth profiles of selected trace elements in sphalerite (a-b) and galena (c-d). See text for explanation.

analyzed each 1½ to 2 h) and converted to concentration values using known Zn content in the analyzed sphalerite as the internal standard. Based on the measured concentrations, the detection limits were calculated for each element in each spot analysis. These values are similar throughout the dataset since consistent spot size would result in comparable count rates for each spot. The error on the element signal is calculated as $(\sigma/\sqrt{n}) \times 100$, where σ = standard deviation and n = number of data points across the selected signal interval. Total analytical error (precision) is expressed as a percentage of concentration and is an expression of analytical noise. The smooth signal profile and good precision obtained for most analysis spots indicate good homogeneity of our samples. In the subsequent sections, we refer to mean analyses (simple numerical means of n individual analyses) for a given element in sphalerite from a specific sample.

5. Results

Trace element composition data of sphalerite (7 samples, 78 spots) and galena (2 samples, 16 spots) from Houdehong are summarized in Table 1. The complete LA-ICP-MS datasets are given in Electronic Appendix A (Supplemental Material1).

5.1. Trace elements in sphalerite

The absolute concentration ranges for selected elements in the Huodehong sphalerite are illustrated in Fig. 4. Published sphalerite data from other Pb-Zn deposit types, including MVT (e.g., Tres Marias (Mexico) and Tennessee (USA); Cook et al., 2009; Bonnet et al., 2016) and carbonate-hosted Pb-Zn deposits in the SYGMP (e.g., Huize; Ye et al., 2011; Tianbaoshan; Ye et al., 2016; Daliangzi; Yuan et al., 2018; Maliping; Hu et al., 2019; Maozu; Li et al., 2020); SEDEX, volcanogenic massive sulfide (VMS) and skarn Pb-Zn deposits (Kelley et al., 2004; Cook et al., 2009; Ye et al., 2011) were also shown in Fig. 4. The median values are used for comparison.

Cadmium is the highest-concentration trace element in our sphalerite samples (495 to 9875 ppm, median 1717 ppm), which can be comparable with that of the Huize deposit, but relatively lower than that of typical MVT deposits and other Pb-Zn deposits (Daliangzi, Tianbaoshan, Maozu and Maliping) in the SYGMP (Fig. 4). Cadmium is uniformly distributed in the sphalerite elemental map (Fig. 5) and displays a smooth LA-ICP-MS time-resolved signal spectra (Fig. 6a-b).

Iron concentration in the sphalerite displays a wide range (85.2 to 6727 ppm, median 882 ppm), which is lower than that of other Pb-Zn deposits (Huize, Daliangzi, Tianbaoshan and Maozu) in the SYGMP and typical SEDEX, VMS, and skarn Pb-Zn deposits, but roughly similar to that of MVT deposits and Maliping deposit in the SYGMP (Fig. 4). Iron, together with Ge, Cd, Zn, and S, shows flat and parallel LA-ICP-MS time-resolved signal profile (Fig. 6a-b), and the elemental map shows relatively homogeneous distribution.

Germanium is the most important by-product commodity in the SYGMP Pb-Zn deposits (Wang, 2010), with its concentration in sphalerite varying over two orders of magnitude (0.86 to 662 ppm, median 139 ppm). Most of our samples have Ge > 60 ppm, slightly above that of the Pb-Zn deposits from the SYGMP and similar to that of MVT deposits, while low levels observed in SEDEX, VMS and skarn Pb-Zn deposits (Fig. 4).

Lead shows a wide concentration range from 1.05 to 4789 ppm (median 879 ppm), and the concentration is comparable with that of

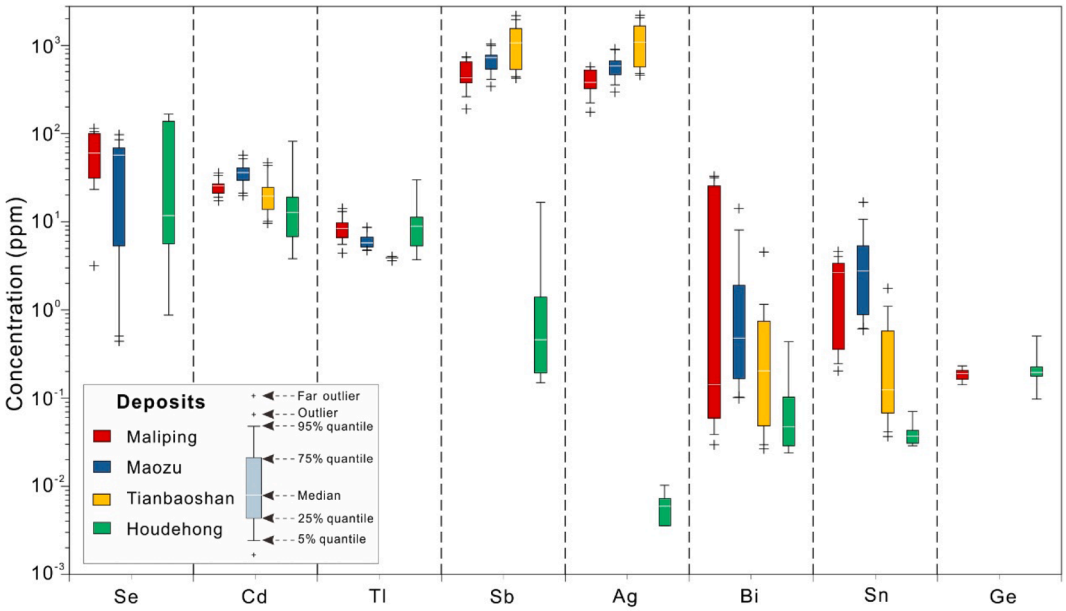

Fig. 7. Box and whisker plots showing trace elements of galena determined by LA-ICPMS from Huodehong and three SYGMP Pb-Zn deposits, i.e., Tianbaoshan (Ye et al., 2016), Maliping (Hu et al., 2019), Maozu (Li et al., 2020).

MVT deposits but higher than that of other genetic types of Pb-Zn deposits shown in Fig. 4. The spike LA-ICP-MS time-resolved signal spectra imply the presence of Pb-bearing micro-inclusions (Fig. 6b).

Thallium concentration ranges from below the detection limit (<0.01 ppm) to 250 ppm, and over half of the analyzed spots are >10 ppm. The Tl concentration is significantly higher than that of the Pb-Zn deposits in the SYGMP, and typical SEDEX, VMS and skarn Pb-Zn deposits worldwide, but is similar to that of MVT deposits (Fig. 4). Thallium content is highly heterogeneous in the elemental map but is relatively smooth and flat in the time-resolved signal profile (Fig. 6a-b).

Manganese concentration in sphalerite varies over two orders of magnitude (1.17 to 376 ppm, median 45.4 ppm). Its variation range is similar to that of MVT and SYGMP Pb-Zn deposits, but significantly lower than that of SEDEX, VMS, and skarn Pb-Zn deposits (Fig. 4).

Copper (0.65 to 183 ppm, median 6.19 ppm) and Ag (1.29 to 24.6 ppm, median 1.88 ppm) contents of the Huodehong sphalerite are among the lowest in the SYGMP Pb-Zn deposits, and lower than those of MVT deposits (Fig. 4).

Cobalt concentration of the Huodehong sphalerite is mostly below the detection limit, and the maximum content (0.16 ppm) is similar to that of the Huize deposit and lower than that of other SYGMP Pb-Zn deposits, MVT, typical SEDEX, VMS and skarn Pb-Zn deposits (Fig. 4).

Nickel (<5.0 ppm), In (<1.0 ppm) and Sn (<14 ppm) concentrations of the Huodehong sphalerite are typically too low to be shown in the LA-ICP-MS time-resolved spectra, and their distribution in the elemental map is highly heterogeneous.

Concentrations of other trace elements, including Sb, As, Se, Te, Mo, W, Pt, and Au, are very low (mostly below the detection limits) in the Huodehong sphalerite (Table 1).

5.2. Trace elements in galena

Concentrations for selected elements in galena from Houdehong, together with published data from the Tianbaoshan (Ye et al., 2016), Maoliping (Hu et al., 2019) and Maozu (Li et al., 2020) Pb-Zn deposits in the SYGMP are illustrated in Fig. 7.

Selenium is the highest-content element in galena, and its concentration varies over two orders of magnitude (0.87 to 166 ppm, median 11.7 ppm). The Se concentration is similar to that of the Pb-Zn deposits (Maliping and Maozu) in the SYGMP (Fig. 7). The time-resolved signal spectra of Ge are smooth and parallel to those of Tl, Pb, and S (Fig. 6c-d).

The Cd (3.79 to 81.2 ppm, median 12.7 ppm) and Tl (3.72 to 29.9 ppm, median 8.87 ppm) concentrations share a similar range to that of many Pb-Zn deposits (Tianbaoshan, Maliping and Maozu) in the SYGMP (Fig. 7). Both elements have smooth and flat LA-ICP-MS time-resolved depth profiles (Fig. 6c-d).

Antimony concentration ranges from below the detection limits (0.1 ppm) to 16.6 ppm (median 0.46 ppm). Its concentration is significantly lower than that of other Pb-Zn deposits (e.g., Tianbaoshan, Maliping and Maozu) in the SYGMP (Fig. 7).

Germanium (0.02 to 0.44 ppm, median 0.05 ppm), Bi (0.17 to 0.50 ppm, 0.04 ppm) and Sn (0.03 to 0.07 ppm, median 0.04 ppm) contents are low (<0.60 ppm) in galena. Both Bi and Sn are slightly lower than those of many SYGMP Pb-Zn deposits (Tianbaoshan, Maliping and Maozu) (Fig. 7). The concentrations are commonly too low to be shown in the LA-ICP-MS time-resolved spectra.

Silver concentrations are only above the detection limits in 6 spots, but their concentrations (<0.01 ppm) are still far below those of many SYGMP Pb-Zn deposits (Tianbaoshan, Maliping and Maozu) (Fig. 7).

Iron and Zn are usually below the detection limit (<0.01 ppm) save a few spots (few ppm). Spot HDH-16-Gn7 contains high concentrations of Fe (349 ppm) and Zn (1075 ppm), and their corresponding spectra display anomalous peaks that suggest Fe- and Zn-bearing micro-inclusions (Fig. 6d).

Concentrations of other elements, including Co, Ni, Cu, As, In, and Te, are below the detection limit in our Houdehong galena samples.

6. Discussion

6.1. Distribution of trace elements in sulfides

Micro-inclusions can be reflected in anomalous peak in the LA-ICP-MS time-resolved signal spectra if they are sufficiently large and heterogeneously distributed in the host minerals (e.g., Cook et al., 2009; Ye et al., 2011, 2016), whereas trace elements in nanoparticles and crystal lattice would show smooth and flat signal spectra (e.g., Gregory et al., 2014; Hu et al., 2020). Trace element mapping and inter-element correlations can provide additional constraint on the trace element occurrence in the host minerals.

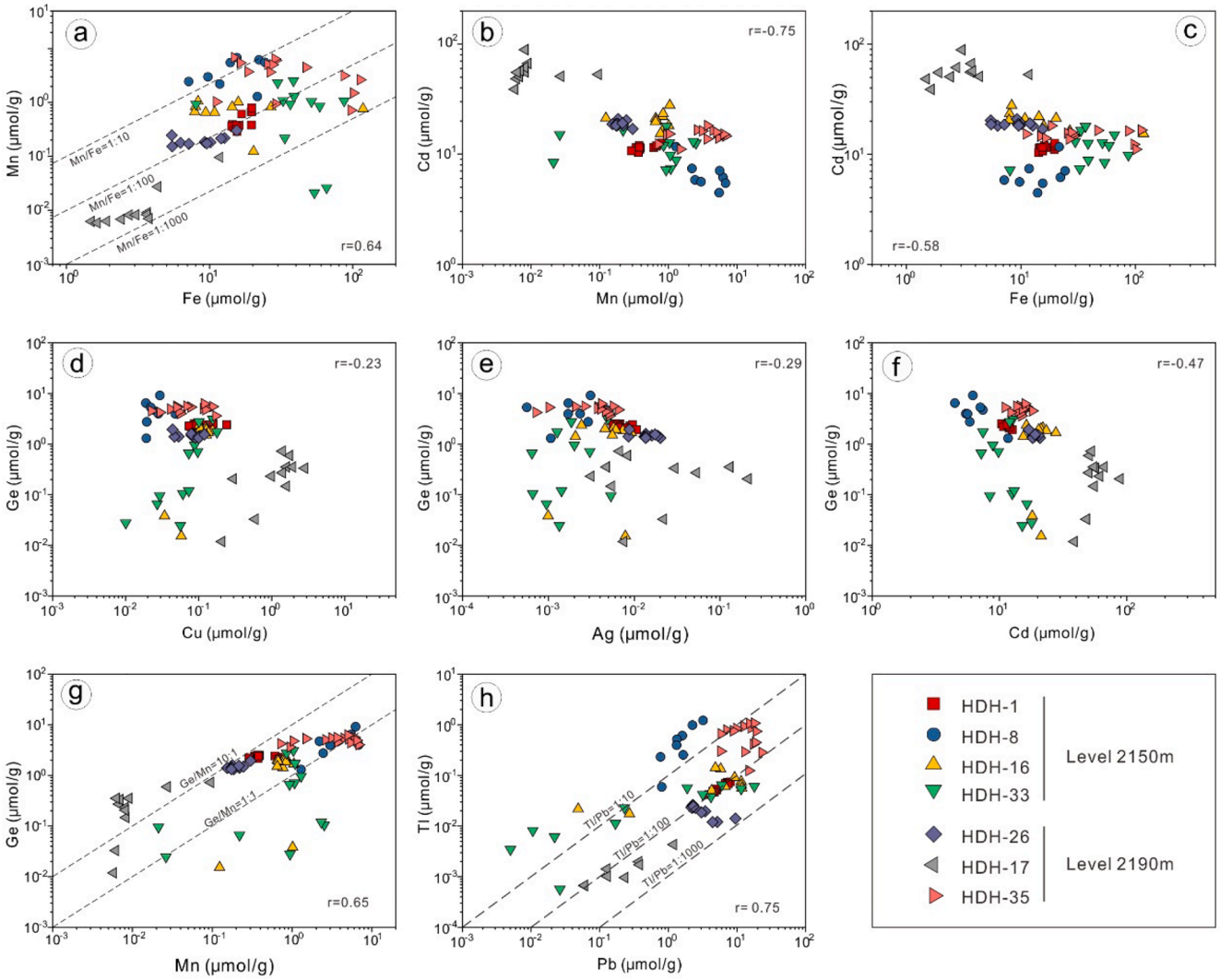

Fig. 8. Binary plots showing inter-element correlation in sphalerite. (a) Fe vs. Mn, (b) Mn vs. Cd, (c) Fe vs. Cd, (d) Cu vs. Ge, (e) Ag vs. Ge, (f) Cd vs. Ge, (g) Mn vs. Ge, and (h) Pb vs. Tl for the Huodehong sphalerite.

6.1.1. Incorporation of trace elements in sphalerite

Many studies have demonstrated that divalent ions (e.g., Cd^{2+}, Fe^{2+}, Mn^{2+}) are incorporated into the sphalerite lattice through directly substituting Zn^{2+} (Di Benedetto et al., 2005; Cook et al., 2009; Ye et al., 2011 and references therein). At Huodehong, the time-resolved depth profiles of these elements are smooth and flat (Fig. 6a-b) and similar to those of Zn and S, suggesting these elements occur as solid solution or homogeneously-distributed nanoparticles. Meanwhile, all spot analyses show that Fe is positively correlate with Mn (r = 0.64; Fig. 8a), but Cd negatively correlated with Mn (r = -0.75; Fig. 8b) and Fe (r = −0.58; Fig. 8c). All these elements are uniformly distributed in their respective elemental maps (Fig. 5). In addition, EMPA results show a strong negative relationship between Zn and Fe + Mn + Cd (r = -0.96). Thus, it is suggested that these divalent elements enter the sphalerite lattice through direct substitution (Zn^{2+}↔ M^{2+}, M = Fe, Mn, Cd; Cook et al., 2009; Ye et al., 2011).

Incorporation of Ge in sphalerite has been investigated in many studies (e.g., Johan, 1988; Cook et al., 2009, 2015; Ye et al., 2011; Wei et al., 2019). Johan (1988) suggested a coupled substitution between tetravalent Ge and a combination of monovalent and divalent Cu ($4Zn^{2+}$↔ Ge^{4+}+ $2Cu^{+}$ + Cu^{2+}) on Ge- and Cu-rich sphalerite from Saint-Salvy (France). Belissont et al. (2014) reported strongly positive Ge vs. Ag correlation in the sphalerite from the Noailhac-Saint-Salvy deposit (France), suggesting that Ge^{4+} enters the sphalerite lattice through the reaction of $3Zn^{2+}$↔ Ge^{4+}+ $2Ag^{+}$. In the SYGMP, previous studies found that the Ge display positive correlation with Cu, together with coordinated change of Ge and Cu in elemental maps, and consequently Ge-Cu coupled substitution for Zn is proposed (e.g., Ye et al., 2016; Wei et al., 2019; Hu et al., 2019; Li et al., 2020). However, our results show that most samples have their Ge concentrations at least two orders of magnitude higher than those of Ag and Cu. Meanwhile, there are no correlation between Cu and Ge (Fig. 8d), or between Ag and Ge (Fig. 8e), indicating that the Ge substitution of Zn in sphalerite could not occur through $4Zn^{2+}$ ↔ $2Cu^{+}$ + Cu^{2+} + Ge^{4+} (Johan 1988), $3Zn^{2+}$ ↔ Ge^{4+} + $2Ag^{+}$ (Belissont et al., 2014), (n + 1) Zn^{2+} ↔ Ge^{2+} + (n + 1) Cu^{2+} (Ye et al., 2016), or $3Zn^{2+}$ ↔ Ge^{4+} + $2Cu^{+}$ (Belissont et al., 2016; Wei et al., 2019). For our Huodehong sphalerite samples, it is noteworthy that Ge has weak negative correlation with Cd (r = -0.47; Fig. 8f) and positive correlation with Mn (r = 0.65; Fig. 8g). Such correlations are also observed in the LA-ICP-MS elemental maps (Fig. 5). Recently, Bonnet et al. (2017) reported X-ray Absorption Near-Edge Structure (XANES) analysis results on the Ge-rich sphalerite from Tennessee (USA), showing that Ge^{4+} and Ge^{2+} coexist in the same sphalerite crystal. Thus, Ge can be incorporated into the sphalerite structure via substitution of Mn^{2+} and Ge^{2+} (or Ge^{4+}) for Zn^{2+} and/or Cd^{2+} ($3(Zn, Cd)^{2+}$ ↔ Ge^{4+} + Mn^{2+} + □ (□ = vacancy)) or $2(Zn, Cd)^{2+}$ ↔ Ge^{2+} + Mn^{2+}).

Table 2
Summary and comparison of MVT, SEDEX, Huodehong and typical Pb-Zn deposits in the SYGMP.

Characteristics	MVT	Huodehong district	Typical Pb-Zn deposits in the SYGMP	SEDEX
Typical deposit/ district	Southeast Missouri land district and Central Tennessee, USA; the Pine Point and Polaris deposit, Canada;	Huodehong deposit	Huize, Maoping and Maozu,	Red dog, USA; Sullivan deposit, Canada; Broken Hill, Australia
Tectonic setting	Carbonates in passive margins in orogenic forelands and rare in the rifts in extensional environments	Yangtze platform carbonate sequences, orogenic thrust belts	Yangtze platform carbonate sequences, orogenic thrust belts	Passive continental margins or Proterozoic rift/Sag basins
Relation with igneous activity	Not associated with igneous activity	Not associated with igneous activity	Close spatial association with the ELIP	Close genetic association with igneous activity, \
Timing of mineralization	Epigenetic (Proterozoic to Cretaceous)	Epigenetic	Epigenetic (225–192 Ma)	Syngeneic to diagenetic (*syn*-sedimentary, early to late burial diagenesis)
Structural controls	Fault, Thrust and fold system and lithology	Faults associated fractures and breccias and lithology	Thrust and fold system and lithology	Syndepositional faults with talus breccias, localized facies variations and/or thickening in sub-basins
Morphology of orebodies	Commonly discordant on a deposit scale but stratabound on a regional scale	Stratiform and/or leneses	Stratiform, lenses, piped and/or veins	Stratiform or strata-bound; commonly in tabular ore bodies
Host rock	Dolostone and limestone, rarely in sandstone	Dolostone	Carbonate rocks (limestone and dolostone)	Mainly shale (siliceous, pyritic, graphitic, carbonaceous or calcareous), coarse clastics (dolomitic siltstones, pyritic siltstones and greywackes)
Ore minerals	Sp, Gn, Py, and Mar (rare)	Sp, Py, Gn,	Sp , Gn, Py, minor Cpy	Sp , Gn, Py, Mar and rare Pyr and Mag
Gangue minerals	Dol, Cal, Fl (rare), Bit (rare), Brt (minor to absent)	Cal and Dol	Dol, Cal, Qtz and Fl (extremely rare), Brt (common)	Qtz (common), Dol, Bar, Sid and Fl (rare)
Ore type	Massive to disseminated, replacement and open-space filling	Massive, disseminated, brecciated, mostly Replacement and open-space filling	Massive sulfide but highly variable and complex textures. mostly replacement, common veins and locally open-space filling	Replacement, disseminated, layered; crusts form sulfides
Ore-forming fluid	Mostly low temperature (90–200 °C) connate bittern brines or evaporite dissolution brines	Low temperature (<180 °C)	Low to moderate temperature (120–280 °C) infiltrated partially evaporated seawater	~120 to ~ 200 °C but possibly to 275 °C (Low silicification: ~ < 200 °C) evaporated seawater
Source of Sulfur	Original Seawater sulfate reduced by a variety of processes and pathways	Evaporitic sulfate reduced by BSR	Evaporitic sulfate reduced by TSR/BSR	Original Seawater sulfate reduced by a variety of processes and pathways
Sources of Pb	Uniform Pb compositions, crustal sources metals	Uniform Pb compositions, metals mainly from Precambrian basement	Uniform Pb compositions, metals from Precambrian basement and country rocks	Uniform Pb compositions, crustal sources of metals
Metal association	Cu, Co, Ni, Ag, Sb, Cd, Ge, Ga, In	Ag, Ga, Ge, Cd	Ge, Ag, Cd, Ga	Ag, Cd, As, Sb, Bi, Hg, In, Tl
References	Leach et al. (2001), Leach et al. (2005)	Jin et al. (2016), Wu et al. (2016), This study	Huang et al. (2004), Han et al. (2007), Zhang et al. (2005), Zhang et al. (2015), Zhou et al. (2018), Li et al. (2020)	Leach et al. (2005)

The Abbreviation: Bit = bitumen; Brt = barite; Cal = calcite; Cpy = chalcopyrite; Dol = dolomite; Gn = galena; Qtz = quartz; Sp = sphalerite; Py = pyrite; Fl = fluorite; Mar = marcasite; OM = oroganic matter; Kfs = potassium feldspar; Pyr = pyrrhotite; Mag = magnetite.

The Pb concentration in sphalerite varies widely, and peaks are found in the LA-ICP-MS time-resolved signal spectra (Fig. 6b), suggesting that Pb may present as micro-inclusion (e.g., galena or other Pb-bearing minerals). Meanwhile, petrographic microscopy (Fig. 3f) and LA-ICP-MS mapping (Fig. 5) show that galena micro-inclusions are present. This conclusion is also supported by the positive Pb vs. Tl correlation in sphalerite (r = 0.75; Fig. 8h), because Tl is preferentially hosted in galena (e.g., George et al., 2015, 2016).

6.1.2. Incorporation of trace elements in galena

For the galena samples, Se, Cd, Tl and Sb display a smooth and flat time-resolved depth profiles (Fig. 6c-d), similar to those of Pb and S. Furthermore, the small standard deviations (Table 1) and the lack of correlation for Zn with Cd, Se, Tl, and Sb all suggest that these elements occur as solid solution in the Huodehong galena, consistent with what George et al. (2015) proposed, or as homogenously-distributed nano-inclusions.

6.2. Anomalously low Ag and Sb in galena

Galena commonly shows wide Ag, Sb and Bi concentration ranges (e.g., Lueth et al., 2000; George et al., 2015 and references therein). Above 420°C, complete solid solution occurs between galena and the two end-members of miargyrite ($AgSbS_2$) and matildite ($AgBiS_2$) (Hoda and Chang, 1975; Sharp and Buseck, 1993). Therefore, coupled substitution of Ag, Bi and Sb into galena represent a well-characterized example of solid solution. However, our Houdehong galena samples have anomalously low Ag (<0.1 ppm) and Sb (mostly < 5 ppm) concentrations, which is significantly lower than those of magmatic-hydrothermal systems (i.e., skarn, VMS and SEDEX; George et al., 2015, 2016), and slightly lower than those of many SYGMP Pb-Zn deposits (e.g., Tianbaoshan, Maliping, and Maozu) (Fig. 4; Ye et al., 2016; Hu et al., 2019; Li et al., 2020). This may have caused by: 1) competition of Sb- and Ag-rich minerals during the galena precipitation; 2) the hydrothermal fluids have very low Sb and Ag concentrations. The second possibility is preferred here. based on the fact that the major hydrothermal minerals at Houdehong (e.g., pyrite, sphalerite, hydrothermal dolomite and calcite) have insignificant influence on the Sb and Ag contents as both elements preferentially partition into galena (e.g., George et al., 2015; Ye et al., 2016; Hu et al., 2019; Wei et al., 2021). Taken the Maoping deposit as an example, the Sb and Ag concentration of galena are up to 2.90 wt% and 0.13 wt% but those in the co-crystallized sphalerite have low concentrations (3.41 ppm of Sb and 84.9 ppm of Ag; Wei et al., 2021). In addition, Sb- and Ag-rich minerals have not been reported in the Houdehong mining area (Jin et al., 2016; Wu et al., 2016). Therefore, the extremely low Sb and Ag in the Houedehong galena may be attributed mainly to the ore-fluid compositions.

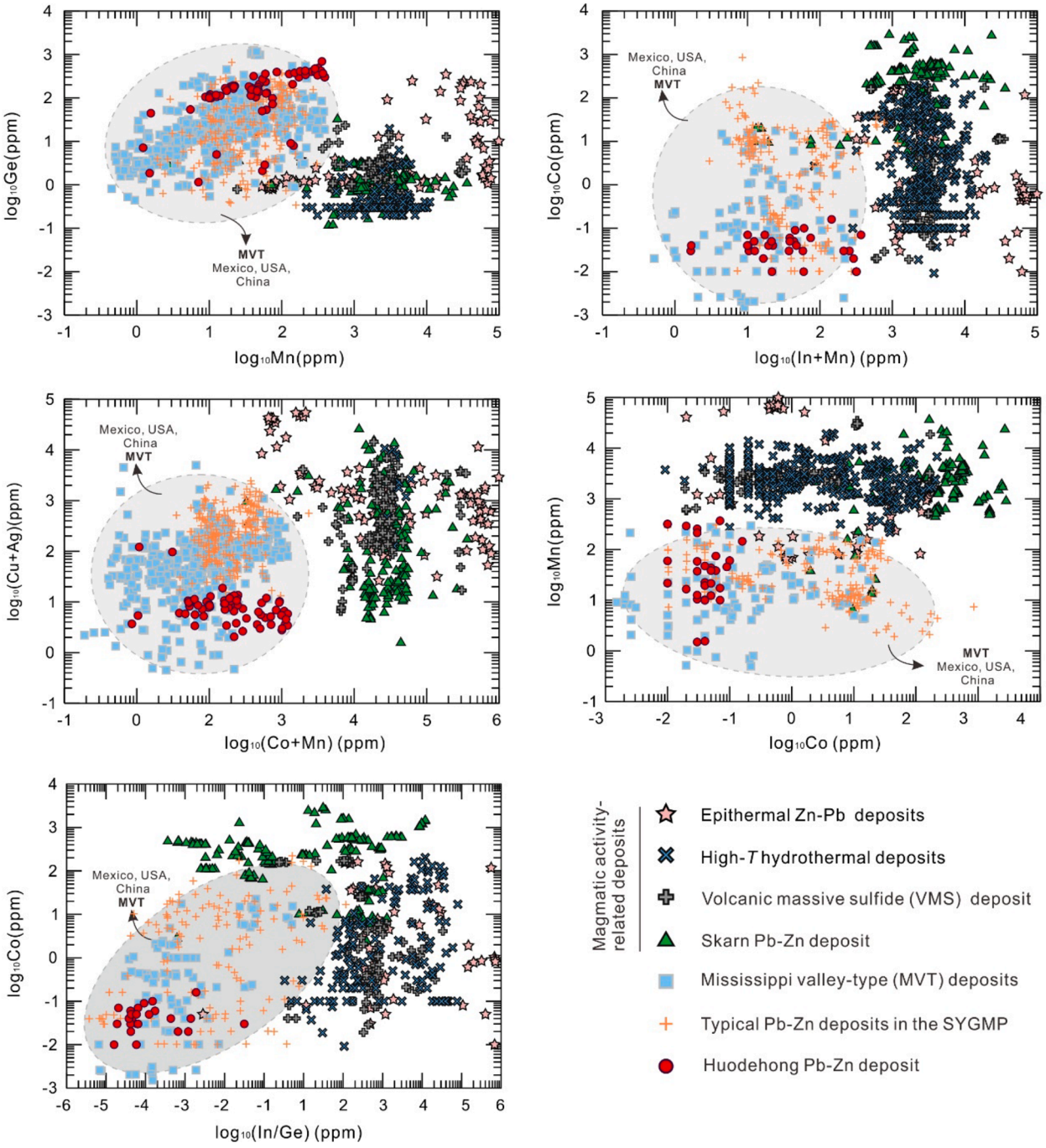

Fig. 9. Binary plots of Mn vs. Ge (a), In + Mn vs. Co (b), Co + Mn vs. Cu + Ag (c), Co vs. Mn (d) and In/Ge vs. Co (e) in sphalerite from the Huodehong and other typical Pb-Zn deposits in SYGMP and MVT, VMS, epithermal, skarn, High-*T* hydrothermal Pb-Zn deposits in China, NE Europe, Canada, USA, Mexico and Japan. Data from Cook et al. (2009), Ye et al. (2011), (Ye et al., 2016), Wei et al. (2019, 2021), Bauer et al. (2018), Yuan et al. (2018), Hu et al. (2019), Li et al. (2020) and Hu (2020).

6.3. Ore-forming temperature

Many studies have demonstrated that the trace element compositions in sphalerite are closely related to the mineralization temperature. In general, high-temperature (high-*T*) sphalerite is featured by high Fe, Mn, Co and In contents with high In/Ge ratio, while high Cd, Ge Ga and Tl contents and low In/Ge ratio are suggestive of low-temperature (low-*T*) sphalerite (e.g., Liu et al., 1984; Ye et al., 2012). As mentioned above, the Huodehong sphalerite is characterized by higher Cd, Ge and Tl but lower Mn, Co and In contents than those of sphalerite from skarn, VMS and SEDEX deposits (Fig. 4). Moreover, the Fe content (85.2–6727 ppm, median 882 ppm) is significantly lower than the marmatite (Fe > 10%) formed under high temperature conditions. Manganese, Co and In contents of the Huodehong sphalerite are also much lower than those of the medium-temperature VMS deposits (e.g., Laochang Pb-Zn polymetallic deposit in China: Mn = 1715–4152 ppm, In = 58–566 ppm, Co > 100 ppm, T = ~250℃; Ye et al., 2012). Moreover, the Huodehong sphalerite In/Ge ratio (4.48×10^{-7}–0.90×10^{-1}, median 0.90×10^{-4}) is distinctly below that of sphalerite from high-*T* magmatic-hydrothermal deposits (e.g., Furong Sn-Zn deposit in China: In/Ge = 2091–16923, T > 350℃; Cai et al., 1996) and medium-temperature deposits (e.g., Laochang Pb-Zn polymetallic deposit: In/Ge = 11–1689; T ~ 250 ℃; Ye

et al., 2012). In addition, the sphalerite GGIMFis (Ga, Ge, In, Mn, and Fe) geothermometer suggested by Frenzel et al. (2016) is used in this study. Although Ga concentration was not analyzed, the Ga concentration (~20 ppm) in sphalerite was estimated according to Ye et al. (2011) and Han et al. (2012). The calculated temperature ranges from 80.4 ℃ to 175.6 ℃ (median 128.1℃), similar to the ore-forming temperature (90–150 °C) of MVT deposits (Leach et al., 2005). Therefore, we suggested that the Hongdehong Pb-Zn mineralization occurred under low temperature conditions.

6.4. Metallogenic implications

Several hypotheses have been proposed for the Pb-Zn metallogenesis in the SYGMP. A great number of authors consider that these Pb-Zn deposits were a syngenetic origin because the orebodies generally show stratigraphic control (e.g., Liu and Lin, 1999; Jin et al., 2016). Several authors have proposed a magmatic hydrothermal model related to ELIP (e.g., Huang et al., 2001; Li et al., 2007; Xu et al., 2014). In contrast, other researchers suggested that these deposits belong to carbonate-hosted deposits associated with the regional compressional tectonic event (e.g., Zhang et al., 2005, 2015; Han et al., 2012; Wu, 2013; Zhou et al., 2018). The Huodehong deposit, one of the typical example of Pb-Zn deposits hosted within the Devonian strata, is similar to these Carboniferous and Sinian-Lower Cambrian dolostone-hosted deposits in term of geologic characteristic, tectonic setting, source of mineralizing material and ore-forming temperature (Table 2), as well as the trace element compositions of sphalerite (Figs. 4 and 9). Therefore, the origin of the Huodehong deposit has significant implications for understanding the Pb-Zn mineralization in the SYG tringle area.

At the Houdehong deposit, the sulfide orebodies are mainly stratiform and lentiform, leading to some authors to proposing a SEDEX or sedimentary reworking-type origin (Liu and Lin, 1999; Jin et al., 2016). However, the ore host lithology and the timing of mineralization are different from that of SEDEX-type (Table 2), which are supported by the galena trace element compositions. For example, the Huodehong galena Bi content (mostly 0.20 ppm) is far below that of SEDEX-type galena (10–1000 ppm; George et al., 2015, 2016). Therefore, the deposit could not be attributed to the syngenetic origin.

Furthermore, trace elements in sphalerite in combination with petrographic description, can be employed to fingerprint different types of ore deposits (Cook et al., 2009; Ye et al., 2011, 2016; Belissont et al., 2014; Wei et al., 2021). A great number of in situ sphalerite trace element studies of Pb-Zn deposits (Ye et al., 2012, 2016; Belissont et al., 2014; Li et al., 2020; Wei et al., 2021) have been published and discussed the significant genetic indication. For example, Cook et al. (2009) noted that trace element endowment of sphalerite can, to a large extent, be correlated with genetic type. Ye et al. (2012) proposed several binary diagrams to discriminate MVT, VMS, magmatic-hydrothermal, and skarn deposits. These discrimination diagrams are useful in identifying the sphalerite with unknown origin. For the Huodehong deposit, in the binary plots of Fig. 9, all samples from Huodehong are plotted significantly far away from the magmatic activity-related (e.g., Epithermal, High-*T* hydrothermal, VMS and skarn) deposit ranges, but overlap with that of the MVT fields, implying that the Huodehong Pb-Zn deposit should be classified as a MVT deposit rather than the hydrothermal deposit related to ELIP.

This viewpoint is also supported by geological and geochemical evidence. As shown in Table 2, the Huodehong deposit is characterized by: (i) epigenetic origin; (ii) sulfide ores in interlayer fractures as cement or replaced oolitic/framboidal diagenetic pyrite; (iii) Pb-Zn mineralization was not related to any intrusive rocks; (iv) simple sulfide mineral assemblage, dominated by sphalerite, pyrite and galena; (v) low-*T* ore-forming fluid (<180℃); (vi) Pb and S isotope results indicate that the metallic elements (e.g., Pb, Zn, etc.) were derived from the Mesoproterozoic basement rocks, and the reduced S was likely sourced from BSR of the Devonian marine sulfates (Jin et al., 2016; Wu et al., 2016). All these geological features are consistent with those of MVT deposits (Table 2; Leach et al., 2005). Therefore, the Huodehong deposit is best attributed to MVT.

7. Conclusions

In this study, we proposed that for the Huodehong sphalerite, divalent cations (Mn^{2+}, Cd^{2+}, and Fe^{2+}) likely entered the sphalerite lattice through direct substitution of Zn^{2+}. Critical element Ge may have entered sphalerite by coupling of Mn^{2+} as 3(Zn, Cd) $^{2+} \leftrightarrow Ge^{4+} + Mn^{2+} + \square$ ($\square$ = vacancy) and 2(Zn, Cd) $^{2+} \leftrightarrow Ge^{2+} + Mn^{2+}$, dependent on the oxidation state of Ge. Lead likely exists in sphalerite as micro-inclusions. The extremely-low Sb and Ag contents of the Huodehong galena may have inherited from the ore-fluid compositions.

Sphalerite from Huodehong is characterized by enrichments in Ge and Tl but depletions in Mn, Co, In and Fe, similar to the sphalerite from MVT deposits. Trace element compositions of the Huodehong sphalerite indicate that the Pb-Zn mineralization occurred under low-temperature conditions (<180℃). The trace element compositional features of sulfides and geological features altogether suggest that the Huodehong deposit is of MVT

Declaration of Competing Interest

The authors declare that they have no known competing financial interests or personal relationships that could have appeared to influence the work reported in this paper.

Acknowledgments

This project was supported by the National Natural Science Foundation of China (41673056 and U1812402), the Key Program of Guizhou Natural Science Foundation ([2017]1421), the State Key Program of National Natural Science Foundation of China (41430315), and National Key R&D Program of China (2017YFC0602500). We would like to thank Drs. Ivan Belousov, Paul Olin, and Sarah Gilbert (CODES, University of Tasmania) for helping with the LA-ICP-MS analysis. The editor Huayong Chen and three anonymous reviewers are indebted for their insightful comments and suggestions.

Appendix A. Supplementary data

Supplementary data to this article can be found online at https://doi.org/10.1016/j.oregeorev.2021.104253.

References

Bauer, M.E., Burisch, M., Ostendorf, J., Krause, J., Frenzel, M., Seifert, T., Gutzmer, J, 2019. Trace element geochemistry of sphalerite in contrasting hydrothermal fluid systems of the Freiberg district, Germany: insights from LA-ICP-MS analysis, near-infrared light microthermometry of sphalerite-hosted fluid inclusions, and sulfur isotope geochemistry. Miner. Deposita 54 (2), 237–262.

Belissont, R., Boiron, M.-C., Luais, B., Cathelineau, M., 2014. LA-ICP-MS analyses of minor and trace elements and bulk Ge isotopes in zoned Ge-rich sphalerites from the Noailhac-Saint-Salvy deposit (France): Insights into incorporation mechanisms and ore deposition processes. Geochim. Cosmochim. Acta 126, 518–540.

Belissont, R., Muñoz, M., Boiron, M.C., Luais, B., Mathon, O., 2016. Distribution and oxidation state of Ge, Cu and Fe in sphalerite by μ-XRF and K-edge μ-XANES: insights into Ge incorporation, partitioning and isotopic fractionation. Geochim. Cosmochim. Acta 177, 298–314.

Bonnet, J., Mosser-Ruck, R., Caumon, M.-C., Rouer, O., Andre-Mayer, A.-S., Cauzid, J., Peiffert, C., 2016. Trace Element Distribution (Cu, Ga, Ge, Cd, and Fe) in Sphalerite from the Tennessee MVT Deposits, USA, By Combined EMPA, LA-ICP-MS, Raman Spectroscopy, and Crystallography. Can. Mineral. 54 (5), 1261–1284.

Bonnet, J., Cauzid, J., Testemale, D., Kieffer, I., Proux, O., Lecomte, A., Bailly, L., 2017. Characterization of Germanium Speciation in Sphalerite (ZnS) from Central and Eastern Tennessee, USA, by X-ray Absorption Spectroscopy. Minerals 7 (5), 79.

Cai, J.H., Zhou, W.N., Zhang, J.Z., 1996. Typomorphic characteristics of sphalerites in the Yinshan copper, lead and zinc polymetallic deposit. Jiangxi. J. Guilin Institute of Tech. 16 (4), 370–375 (in Chinese with English abstract).

Ciobanu, C.L., Cook, N.J., Kelson, C.R., Guerin, R., Kalleske, N., Danyushevsky, L., 2013. Trace element heterogeneity in molybdenite fingerprints stages of mineralization. Chem. Geol. 347, 175–189.
Cook, N.J., Ciobanu, C.L., Pring, A., Skinner, W., Shimizu, M., Danyushevsky, L., Saini-Eidukat, B., Melcher, F., 2009. Trace and minor elements in sphalerite: A LA-ICP-MS study. Geochim. Cosmochim. Acta 73 (16), 4761–4791.
Cook, N.J., Sundblad, K., Valkama, M., Nygård, R., Ciobanu, C.L., Danyushevsky, L., 2011. Indium mineralisation in A-type granites in southeastern Finland: Insights into mineralogy and partitioning between coexisting minerals. Chem. Geol. 284 (1-2), 62–73.
Cook, N., Etschmann, B., Ciobanu, C., Geraki, K., Howard, D., Williams, T., Rae, N., Pring, A., Chen, G., Johannessen, B., Brugger, J., 2015. Distribution and substitution mechanism of Ge in a Ge-(Fe)-bearing sphalerite. Minerals 5 (2), 117–132.
Danyushevsky, L., Robinson, P., Gilbert, S., Norman, M., Large, R., McGoldrick, P., Shelley, M., 2011. Routine quantitative multi-element analysis of sulphide minerals by laser ablation ICP-MS: Standard development and consideration of matrix effects. Geochem. Explor. Environ. Anal. 11 (1), 51–60.
Di Benedetto, F., Bernardini, G.P., Costagliola, P., Plant, D., Vaughan, D.J., 2005. Compositional zoning in sphalerite crystals. Am. Mineral. 90, 1384–1392.
Frenzel, M., Hirsch, T., Gutzmer, J., 2016. Gallium, germanium, indium, and other trace and minor elements in sphalerite as a function of deposit type - A meta-analysis. Ore Geol. Rev. 76, 52–78.
Gregory, D., Meffre, S., Large, R., 2014. Comparison of metal enrichment in pyrite framboids from a metal-enriched and metal-poor estuary. Am. Mineral. 99 (4), 633–644.
George, L.L., Cook, N.J., Ciobanu, C.L., 2016. Partitioning of trace elements in co-crystallized sphalerite-galena- chalcopyrite hydrothermal ores. Ore Geol. Rev. 77, 97–116.
George, L., Cook, N.J., Ciobanu, C.L., Wade, B.P., 2015. Trace and minor elements in galena: A reconnaissance LA-ICP-MS study. Am. Mineral. 100 (2-3), 548–569.
Han, R.-S., Liu, C.-Q., Huang, Z.-L., Chen, J., Ma, D.-Y., Lei, L.i., Ma, G.-S., 2007. Geological features and origin of the Huize carbonate-hosted Zn-Pb-(Ag) District, Yunnan. South China. Ore Geol. Rev. 31 (1-4), 360–383.
Han, R.S., Hu, Y.Z., Wang, X.K., Hou, B.H., Huang, Z.L., Chen, J., Wang, F., Wu, P., Li, B., Wang, H.J., Dong, Y., Lei, L., 2012. Mineralization model of rich Ge–Ag-bearing Zn–Pb polymetallic deposit concentrated district in northeastern Yunnan. China. Acta. Geol. Sin-Engl. 86, 280–294 (in Chinese with English abstract).
Hoda, S.N., Chang, L.L.Y., 1975. Phase relations in the systems PbS-Ag_2S-Sb_2S_3 and PbS-Ag_2S-Bi_2S_3. Am. Mineral. 60, 621–633.
Hu, R.Z., Zhou, M.F., 2012. Multiple Mesozoic mineralization events in South China an introduction to the thematic issue. Miner. Deposita 47 (6), 579–588.
Hu, Y.S., Ye, L., Huang, Z.L., Li, Z.L., Wei, C., Danyushevsky, L., 2019. Distribution and existing forms of trace elements from Maliping Pb-Zn deposit in Northeastern Yunnan, China: A LA-ICPMS study. Acta Petrol. Sin. 35 (11), 3477–3492 (in Chinese with English abstract).
Hu, Y.S., Ye, L., Wei, C., Li, Z.L., Huang, Z.L., Wang, H.Y., 2020. Trace elements in sphalerite from the Dadongla Zn-Pb deposit, western Hunan−Eastern Guizhou Zn-Pb metallogenic belt. South China. Acta. Geol. Sin-Engl. 94 (6), 2152–2164.
Hu, Y.S., 2020. The metallogenesis of Pb-Zn deposits hosted in Cambrian carbonate from Western Hunan-Eastern Guizhou base metal metallogenic belt, China. Ph.D. Dissertation. University of Chinese Academy of Sciences, pp. 1–161 (in Chinese with English Abstract).
Huang, Z.L., Chen, J., Han, R.S., Li, W.B., Liu, C.Q., Zhang, Z.L., Ma, D.Y., Gao, D.R., and Yang, H.L., 2004. Geochemistry and Ore Genesis of the Huize Giant Pb-Zn Deposit in Yunnan Province, China: Discussion on the Relationship between the Emeishan Flood Basalts and Pb-Zn Mineralization. Geological Publishing House, Beijing, pp. 1–214 (in Chinese).
Huang, Z.L., Chen, J., Liu, C.Q., Han, R.S., Li, W.B., Zhao, D.S., Gao, D.R., Feng, Z.B., 2001. A preliminary discussion on the genetic relationship between Emeishan basalts and Pb-Zn deposits as exemplified by the Huize Pb-Zn deposit. Yunnan province. Acta Mineral. Sin. 21, 681–688 (in Chinese with English abstract).
Jin, C.H., Zhang, Y., Shen, Z.W., Zhang, D., 2016. Geological characteristics and metallogenic material source of the Huodehong Pb-Zn deposit, northeast Yunnan province. J. Mineral. Petrol. 36 (4), 50–56 (in Chinese with English abstract).
Johan, Z., 1988. Indium and germanium in the structure of sphalerite: an example of coupled substitution with copper. Miner. Petrol. 39, 211–229.
Kelley, K.D., Leach, D.L., Johnson, C.A., Clark, J.L., Fayek, M., Slack, J.F., Anderson, V. M., Ayuso, R.A., Ridley, W.I., 2004. Textural, compositional, and sulfur isotope variations of sulfide minerals in the Red Dog Zn-Pb-Ag deposits, Brooks Range, Alaska: implications for ore formation. Econ. Geol. 99 (7), 1509–1532.
Leach, D.L., Bradley, D., Lewchuk, M.T., Symons, D.T., de Marsily, G., Brannon, J., 2001. Mississippi Valley-type lead-zinc deposits through geological time: Implications from recent age-dating research. Miner. Deposita 36 (8), 711–740.
Leach, D.L., Sangster, D.F., Kelley, K.D., Large, R.R., Garven, G., Allen, C.R., Gutzmer, J., Walters, S., 2005. Sediment-hosted lead-zinc deposits: A global perspective. Econ. Geol. 100th Anniv, 561–607.
Lueth, V.W., Megaw, P.K.M., Pingitore, N.E., Goodell, P.C., 2000. Systematic Variation in Galena Solid-Solution Compositions at Santa Eulalia, Chihuahua. Mexico. Econ. Geol. 95 (8), 1673–1687.
Li, W.B., Huang, Z.L., Yin, M.D., 2007. Dating of the giant Huize Zn-Pb ore field of Yunnan province, southwest China: constrains from the Sm-Nd system in hydrothermal calcite. Resour. Geol. 57, 90–97.
Li, Z.L., Ye, L., Hu, Y.S., Wei, C., Huang, Z.L., Yang, Y.L., Danyushevsky, L., 2020. Trace elements in sulfides from the Maozu Pb-Zn deposit, Yunnan Province, China: Implications for trace-element incorporation mechanisms and ore genesis. Amer. Mineral. 105, 1734–1751.
Lin, Z.Y., Wang, D.H., Zhang, C.Q., 2010. Rb-Sr isotopic age of sphalerite from the Paoma lead-zinc deposit in Sichuan Province and its implications. Geol. China 37, 488–1196 (in Chinese with English abstract).
Liu, Y.J., Cao, L.M., Li, Z.L., Wang, H.L., Chu, T.Q., Zhang, J.R., 1984. Element Geochemistry. Geological Publishing House, Beijing, pp. 1–548 (in Chinese).
Liu, H.C., Lin, W.D., 1999. The ore-forming regularity of lead, zinc, and silver deposits in northeastern Yunnan province. University of Yunnan Press, Kunming, pp. 1–468 (in Chinese).
Sharp, T.G., Buseck, P.R., 1993. The distribution of Ag and Sb in galena; inclusions versus solid solution. Amer. Mineral. 78, 85–95.
Wang, F., 2010. Analysis of metallogenic regularity and resources potential of lead-zinc polymetallic ore zone in northeast Yunnan province. Yunnan. Metall. 39(4), 3–7, 49 (in Chinese with English abstract).
Wei, C., Ye, L., Hu, Y.S., Danyushevsky, L., Li, Z.L., Huang, Z.L., 2019. Distribution and occurrence of Ge and related trace elements in sphalerite from the Lehong carbonate-hosted Zn-Pb deposit, northeastern Yunnan, China: Insights from SEM and LA-ICP-MS studies. Ore Geol. Rev. doi.org/10.1016/j.oregeorev.2019 .103175.
Wei, C., Ye, L., Hu, Y., Huang, Z., Danyushevsky, L., Wang, H., 2021. LA-ICP-MS analyses of trace elements in base metal sulfides from carbonate-hosted Zn-Pb deposits, South China: A case study of the Maoping deposit. Ore Geol. Rev. 130, 103945. https://doi.org/10.1016/j.oregeorev.2020.103945.
Wu, Y., 2013. The age and ore-forming process of MVT deposits in the boundary area of Sichuan-Yunnan-Guizhou province, southwest China. Ph.D. Dissertation. Beijing, China University of Geosciences, pp. 1–167 (in Chinese).
Wu, Y.D., Wang, Z.Q., Luo, J.H., Chen, J.X., Zhang, Y.L., Wang, S.D., 2016. Geochemical characteristics and metallogenic mechanism analysis of Huodehong lead-zinc deposit, northeast Yunnan Province. Mineral Depos. 35 (5), 1084–1098 (in Chinese with English abstract).
Xiong, S.F., Gong, Y.J., Jiang, S.Y., Zhang, X.J., Li, Q., Zeng, G.P., 2018. Ore genesis of the Wusihe carbonate-hosted Zn-Pb deposit in the Dadu River Valley district, Yangtze Block, SW China: evidence from ore geology, S-Pb isotopes, and sphalerite Rb-Sr dating. Miner. Deposita 53 (7), 967–979.
Xu, Y., Huang, Z., Zhu, D., Luo, T., 2014. Origin of hydrothermal deposits related to theEmeishan magmatism. Ore Geol. Rev. 63, 1–8.
Yan, D.P., Zhou, M.F., Song, H., Fu, Z., 2003. Structural style and tectonic significance of the Jianglang dome in the eastern margin of the Tibetan Plateau. China. J. Struct. Geol. 25 (5), 765–779.
Ye, L., Cook, N.J., Ciobanu, C.L., Yuping, L., Qian, Z., Tiegeng, L., Wei, G., Yulong, Y., Danyushevskiy, L., 2011. Trace and minor elements in sphalerite from base metal deposits in South China: a LA-ICPMS study. Ore Geol. Rev. 39 (4), 188–217.
Ye, L., Gao, W., Yang, Y.L., Liu, T.G., Peng, S.S., 2012. Trace elements in sphalerite in Laochang Pb-Zn polymetallic deposit, Lancang. Yunnan Province. Acta Petrol. Sin. 28 (5), 1362–1372 (in Chinese with English abstract).
Ye, L., Li, Z.L., Hu, Y.S., Huang, Z.L., Zhou, J.X., Fan, H.F., Danyushevsky, L., 2016. Trace elements in sulfide from the Tianbaoshan Pb-Zn deposit, Sichuan Province, China: A LA-ICPMS study. Acta Petrol. Sin. 32 (11), 3377–3393 (in Chinese with English abstract).
Yuan, Bo., Zhang, C., Yu, H., Yang, Y., Zhao, Y., Zhu, C., Ding, Q., Zhou, Y., Yang, J., Xu, Y., 2018. Element enrichment characteristics: Insights from element geochemistry of sphalerite in Daliangzi Pb-Zn deposit, Sichuan. Southwest China. J Geochem. Explor. 186, 187–201.
Zhang, C.Q., Mao, J.W., Wu, S.P., Li, H.M., Liu, F., Guo, B.J., Gao, D.R., 2005. Distribution characteristics and genesis of Mississippi Valley-Type lead-zinc deposits in Sichuan-Yunnan-Guizhou area. Mineral Depos. 24 (3), 336–348 (in Chinese with English abstract).
Zhang, C., Wu, Y., Hou, L., Mao, J., 2015. Geodynamic setting of mineralization of Mississippi Valley-type deposits in world-class Sichuan-Yunnan-Guizhou Zn-Pb triangle, southwest China: Implications from age-dating studies in the past decade and the Sm-Nd age of Jinshachang deposit. J. Asian Earth Sci. 103, 103–114.
Zhou, J.X., Huang, Z.L., Yan, Z.F., 2013a. The origin of the Maozu carbonate-hosted Pb-Zn deposit, southwest China: constrained by C-O-S-Pb isotopic compositions and Sm-Nd isotopic age. J. Asian Earth Sci. 73, 39–47.
Zhou, J., Huang, Z., Zhou, M., Li, X., Jin, Z., 2013b. Constraints of C-O–S–Pb isotope compositions and Rb–Sr isotopic age on the origin of the Tianqiao carbonate-hosted Pb–Zn deposit. SW China. Ore Geol. Rev. 53, 77–92.
Zhou, J.X., Xiang, Z.Z., Zhou, M.F., Feng, Y.X., Luo, K., Huang, Z.L., Wu, T., 2018. The giant Upper Yangtze Pb–Zn province in SW China: Reviews, new advances and a new genetic model. J. Asian Earth Sci. 154, 280–315.